




Solitary Pulmonary Inflammatory Nodule: CT Features and Pathological Findings

Yun-Dan Xiao*

Fa-Jin Lv*

Wang-Jia Li Bin-Jie Fu 

Rui-Yu Lin

Zhi-Gang Chu 

Department of Radiology, The First
Affiliated Hospital of Chongqing Medical
University, 1# Youyi Road, Yuanjiagang,
Yuzhong District, Chongqing, People's Republic
of China

*These authors contributed equally to
this work

Purpose: Solitary pulmonary inflammatory nodules (SPINs) are frequently misdiagnosed as malignancy. We aimed to investigate CT features and pathological findings of SPINs for improving diagnosis strategies.

Patients and Methods: In this retrospective study, 225 and 310 consecutive patients with confirmed SPINs and lung cancerous nodules were enrolled from January 2013 to December 2020. Nodules were classified into different types based on the key CT features: I, homogeneous and well-defined nodules with smooth (Ia), coarse (Ib), or spiculated margins (Ic); II, nodules with blurred boundaries, peripheral patches, or both; III, nodules exhibiting heterogeneous density; and IV, polygonal nodules. The pathological findings of SPINs were simultaneously studied and summarized.

Results: Among the 225 SPINs, type I (Ia, Ib, and Ic), II, III, and IV were 137 (60.9%) (47 [20.9%], 33 [14.7%], and 57 [25.3%]), 62 (27.6%), 12 (5.3%) and 14 (6.2%), respectively. Correspondingly, those in 310 cancerous nodules were 275 (88.7%) (119 [38.4%], 70 [22.6%], and 86 [27.7%]), 20 (6.5%), 15 (4.8%), and 0, respectively. Compared with lung cancers, type I nodules were less common but type II and IV nodules were more common in SPINs (each $P < 0.0001$). Though the frequencies of subtype I ($P = 0.095$) and type III ($P = 0.796$) nodules were similar between two groups, their specific CT features were significantly different. The main pathological findings of each type of SPINs were most extensively identical (82.2 – 100%).

Conclusion: Between cancerous nodules and SPINs, differences in overall or specific CT features exist. The type II and IV nodules are highly indicative of SPINs, and each type of SPINs have almost similar pathological findings.

Keywords: solitary pulmonary nodule, tomography, X-ray computed, inflammation, CT-pathology correlation

Introduction

Solitary pulmonary nodules are usually detected incidentally or during screening for lung cancer.^{1,2} Solitary pulmonary nodules arise mainly from tumors (benign or malignant), infectious lesions, and noninfectious lesions.^{2,3} The treatment and prognosis for benign nodules differ significantly from those for malignant nodules.^{3–7} Therefore, accurate diagnosis of pulmonary nodules is of great importance in clinical practice. Currently, computed tomographic (CT) scanning is the best diagnostic imaging tool for pulmonary nodules. However, benign and malignant nodules have many similar CT features.^{2,4–7} For example, most well-defined solitary pulmonary nodules with smooth margins have been benign, but 21% of malignant nodules also shared such features.^{2,8} Thus, distinguishing their CT characteristics of benign and malignant nodules is of great significance.

Correspondence: Zhi-Gang Chu
Department of Radiology, The First
Affiliated Hospital of Chongqing Medical
University, 1# Youyi Road, Yuanjiagang,
Yuzhong District, Chongqing, 400016,
People's Republic of China
Tel +86 18723032809
Fax +86 23 68811487
Email chuzg0815@163.com

Solitary pulmonary nodules may be solid or subsolid. Previous studies had confirmed that ground-glass nodules, especially the mixed ones, had an extremely high probability of being malignant.^{9–12} However, the pathological nature of solid nodules is diverse, correctly differentiating them is crucial but difficult. In fact, a confident diagnosis of benignity can be made only for completely calcified or fat-containing nodules.¹³ The majority of incidental and screen-detected pulmonary solid nodules are inflammatory lesions (both healed and active) and benign tumors.¹³ CT manifestations of pulmonary benign tumors are usually similar, whereas those of inflammatory nodules and lung cancers are often complex, and such lesions need to be further understood and distinguished.

Previous studies have focused on differentiating all kinds of benign and malignant pulmonary nodules,^{14–16} but no study specifically for the CT manifestations of solitary pulmonary inflammatory nodules (SPINs) has been reported. Furthermore, we have found no report about the systematic correlation between CT features and pathological findings of SPINs. The aim of this study was to summarize and clarify the CT features of SPINs by comparing inflammatory and cancerous nodules. In addition, the pathological characteristics of SPINs were studied for better understanding their CT findings.

Patients and Methods

Patients

This retrospective observational study was conducted in the First Affiliated Hospital of Chongqing Medical University between January 2013 and December 2020 in China. Patients with surgically resected (video-assisted thoracic surgery segmentectomy or lobectomy) and pathologically confirmed SPINs (main pathological findings included inflammatory cells infiltration and fibrous tissue proliferation) and lung cancers were consecutively enrolled in this study. All the patients underwent chest CT examination within a week before surgery. Inclusion criteria were as follows: (1) The lesion was a nodule (diameter, ≤ 3 cm); (2) the lesion was solid; and (3) the patients' clinical and pathological data were complete. The exclusion criterion was CT images containing breath artifact. In all, 225 patients with SPINs and 310 cases with lung cancers were enrolled in this study.

CT Protocol

All studies were performed on a SOMATOM Definition Flash CT scanner (Siemens Healthineers, Erlangen,

Germany) with following parameters for non-contrast chest scan: 120 kV, 100 mAs, rotation time of 0.5 s, pitch of 1, 128×0.6 mm collimation, and 5-mm slice thickness and 5-mm interval for axial images. During CT examination, all the patients were uniformly scanned in the craniocaudal direction and placed in a supine position with both hands placed near the head. The scanning range included the whole chest from the level of the thoracic inlet to immediately below the costophrenic angle. Contiguous transverse images were reconstructed with a slice thickness of 0.6 mm and a standard filtered back projection algorithm involving a kernel of high spatial resolution (lung images: widths of 1200–1600 HU and levels of –500–700 HU) and a soft-tissue kernel (mediastinal images: widths of 350–450 HU and levels of 20–40 HU), respectively.

Image and Pathological Findings Analysis

All patients' CT data were initially reviewed on a workstation (Advantage Workstation 4.6; GE Healthcare, Chicago) by two senior chest radiologists (reviewer 1 has 12 years of experience, reviewer 2 has 25 years of experience) who were unaware of the pathological results of the nodules. Interpretation discrepancy, if any, was resolved by consensus.

On CT image, the following characteristics were evaluated: nodule distribution in different lobes, lesion size (mean of the longest diameter and perpendicular diameter on axial images), locations (whether abutting pleura or not, wide or narrow base connected to pleura), shape (round, oval, polygonal, or irregular), nodule–lung interface (well-defined or blurred), margins (smooth, coarse, or spiculated), density on lung window images (homogeneous or heterogeneous), internal signs (calcification, cavity, vacuole, and air bronchogram), and changes in the surrounding lung field (clear, patchy, or fibrotic). Wide base indicated the diameter of nodule–pleura contact surface was greater than or equal to that of nodule, or it was narrow base. Peripheral patch indicated that there was ground glass opacity surrounding nodules or locating at one side. Spiculation was further described as intensive if spiculations densely distributed around the nodules or as sparse, and short (length of spiculation \leq diameter of nodule) or long (length of spiculation $>$ diameter of nodule).

Based on the key CT features (order of categorization basis: shape [polygonal or not], density [heterogeneous or not], boundary [blurred or not], changes in peripheral lung

fields [peripheral patch or not], and margin [smooth, coarse, or spiculated]), nodules were classified into different types: I, homogeneous and well-defined nodules with smooth (Ia), coarse (Ib), or spiculated margins (Ic); II, nodules with blurred boundaries, peripheral patches, or both; III, nodules exhibiting heterogeneous density; and IV, polygonal nodules.

The pathological findings of nodules were reviewed and summarized by pathologist with 10 years of experience. The main pathological components were determined for each type of SPINs.

Statistical Analysis

Patients' clinical data and CT features of nodules were statistically analyzed. Continuous variables were expressed as means \pm standard deviations, whereas categorical variables were expressed as absolute numbers and percentages. Statistical differences were analyzed using the Wilcoxon rank sum test for patient age and mean diameter of nodules. Patients' clinical data, types of nodules on CT images, and CT features of nodules were compared between two groups by using the Pearson χ^2 test and Fisher exact test, as appropriate. The κ statistic was used to calculate the interobserver variability in classifying nodules. Statistical analysis was performed with the SPSS 20.0 software package (IBM, Chicago). A p value of less than 0.05 was considered significant.

Results

Study Population

Patients' clinical data are summarized in Table 1. Compared with patients with lung cancers, those with SPINs were younger ($P < 0.0001$), and there were less smokers ($P = 0.033$), less cases with symptoms ($P = 0.001$) but more with pulmonary basic diseases ($P < 0.0001$).

Types of SPINs and Lung Cancers on CT Images

Numbers of nodules distributed in the upper, middle, and lower lobe of right lung and upper and lower lobe of left lung were 83 (36.9%), 19 (8.4%), 54 (24.0%), 39 (17.3%) and 30 (13.3%) and 106 (34.2%), 30 (9.7%), 51 (16.5%), 74 (23.9%), and 49 (15.8%) in SPIN and lung cancer groups, respectively. Of the 225 SPINs (mean diameter: 14.7 ± 6.3 mm, range: 4–30 mm) and 310 lung cancers (mean diameter: 17.3 ± 6.5 mm, range: 4–30 mm), 155

Table 1 Patients' Clinical Data

	Patients with SPINs (n = 225)	Patients with Lung Cancers (n = 310)	P-values
Age (years)	55.3 \pm 10.4	61.4 \pm 9.8	< 0.0001
Men/women	138/87	171/139	0.154
Smokers	83 (36.9)	143 (46.1)	0.033
Clinical symptoms	82 (36.4)	159 (51.3)	0.001
Cough	47 (57.3)	143 (89.9)	< 0.0001
Expectoration	39 (47.6)	120 (75.5)	< 0.0001
Chest pain	27 (32.9)	35 (22.0)	0.066
Phlegm with blood	14 (17.1)	23 (14.5)	0.595
Hemoptysis	6 (7.3)	10 (6.3)	0.761
Fever	3 (3.7)	7 (4.4)	1.000
Pulmonary basic diseases	57 (25.3)	35 (11.3)	< 0.0001
Chronic inflammation	26 (45.6)	13 (37.1)	0.425
COPD	22 (38.6)	14 (40.0)	0.893
Tuberculosis	9 (15.8)	9 (25.7)	0.244
Bronchial asthma	2 (3.5)	2 (5.7)	1.000

Note: Data are expressed as n (%).

(68.9%) and 271 (87.4%) were round or oval, 14 (6.2%) and 0 were polygonal, and 56 (24.9%) and 39 (12.6%) were irregular, respectively. The lobulated sign was detected 141 (45.5%) lung cancers and 32 (14.2%) SPINs. Compared with lung cancerous nodules, the SPINs were smaller ($P < 0.0001$), more irregular ($P < 0.0001$), and less lobulated ($P < 0.0001$).

The classifications of SPINs and lung cancers based on key CT features are shown in Tables 2 and 3, respectively. There was perfect agreement between the two observers on classifying SPINs ($\kappa = 0.908$) and lung cancers ($\kappa = 0.924$). Among the 225 SPINs, type I (Ia, Ib, and Ic) nodules were 137 (60.9%) (47 [20.9%], 33 [14.7%], and 57 [25.3%]), 62, (27.6%), 12 (5.3%) and 14 (6.2%), respectively. Correspondingly, type I (Ia, Ib, and Ic) (Figure 5A–D), II (Figure 5E and F), III (Figure 5G and H), and IV in lung cancer group were 275 (88.7%) (119 [38.4%], 70 [22.6%], and 86 [27.7%]), 20 (6.5%), 15 (4.8%), and 0, respectively. Compared with lung cancers, type I nodules were less common ($P < 0.0001$) but type II

Table 2 Classification of SPINs Based on Key CT Features

Types	Numbers	Calcification	Vacuole or Cavity	Spiculation	Peripheral Patch	Abutting Pleura	Wide Base with Pleura	Pleural Indentation	Sporadic Patch in Same Lobe	Air Bronchogram
I: Well-defined boundary	137 (60.9)	8 (5.8)	7 (5.1)			32 (23.4)	26 (19.0)	11 (8.0)	13 (9.5)	4 (2.9)
la: Smooth margin	47 (34.3)	3 (6.4)	2 (4.3)	-	-	17 (36.2)	11 (23.4)	2 (4.3)	2 (4.3)	-
lb: Coarse margin	33 (24.1)	-	4 (12.1)	-	-	7 (21.2)	9 (27.3)	2 (6.1)	2 (6.1)	1 (3.0)
lc: Spiculated margin	57 (41.6)	5 (8.8)	1 (1.8)	/	-	8 (14.0)	6 (10.5)	7 (12.3)	9 (15.8)	3 (5.3)
II: Blurred boundary/ Peripheral patch	62 (27.6)	1 (1.6)	6 (9.7)	10 (16.1)		21 (33.9)	14 (22.6)	5 (8.1)	11 (17.7)	2 (3.2)
Blurred boundary	34 (54.8)	1 (2.9)	3 (8.8)	7 (20.6)	-	11 (32.4)	5 (14.7)	1 (2.9)	5 (14.7)	1 (2.9)
Peripheral patch	28 (45.2)	-	3 (10.7)	3 (10.7)	/	10 (35.7)	9 (32.1)	4 (14.3)	6 (21.4)	1 (3.6)
III: Heterogeneous nodules	12 (5.3)	-	-	6 (50.0)	1 (8.3)	1 (8.3)	-	6 (50.0)	2 (16.7)	3 (25.0)
IV: Polygonal nodules	14 (6.2)	2 (14.3)	1 (7.1)	2 (14.3)	1 (7.1)	4 (28.6)	1 (7.1)	1 (7.1)	3 (21.4)	-
Total	225	11 (4.9)	14 (6.2)	18 (8.0)	2 (0.9)	58 (25.8)	41 (18.2)	23 (10.2)	29 (12.9)	9 (4.0)

Note: Data are express as n (%).

Table 3 Classification of Lung Cancers Based on Key CT Features

Types	Numbers	Calcification	Vacuole or Cavity	Spiculation	Peripheral Patch	Abutting Pleura	Wide Base with Pleura	Pleural Indentation	Sporadic Patch in Same Lobe	Air Bronchogram
I: Well-defined boundary	275 (88.7)	4 (1.5)	24 (8.7)			11 (4.0)	6 (2.2)	29 (10.5)	13 (4.7)	10 (3.6)
la: Smooth margin	119 (43.3)	-	7 (5.9)	-	-	7 (5.9)	3 (2.5)	8 (6.7)	2 (1.7)	3 (2.5)
lb: Coarse margin	70 (25.5)	-	5 (7.1)	-	-	4 (5.7)	3 (4.3)	7 (10.0)	5 (7.1)	1 (1.4)
lc: Spiculated margin	86 (31.3)	4 (4.7)	12 (14.0)	/	-	-	-	14 (16.3)	6 (7.0)	6 (7.0)
II: Blurred boundary/ Peripheral patch	20 (6.5)			5 (25.0)				2 (10.0)		
Blurred boundary	2 (10.0)	-	-	-	-	-	-	1 (50.0)	-	-
Peripheral patch	18 (90.0)	-	-	5 (27.8)	/	-	-	1 (5.6)	-	-
III: Heterogeneous nodules	15 (4.8)	-	-	1 (6.7)	-	-	-	-	-	1 (6.7)
IV: Polygonal nodules	-	-	-	-	-	-	-	-	-	-
Total	310	4 (1.3)	24 (7.7)	6 (1.9)	-	11 (3.5)	6 (1.9)	31 (10.0)	13 (4.2)	11 (3.5)

Note: Data are express as n (%).

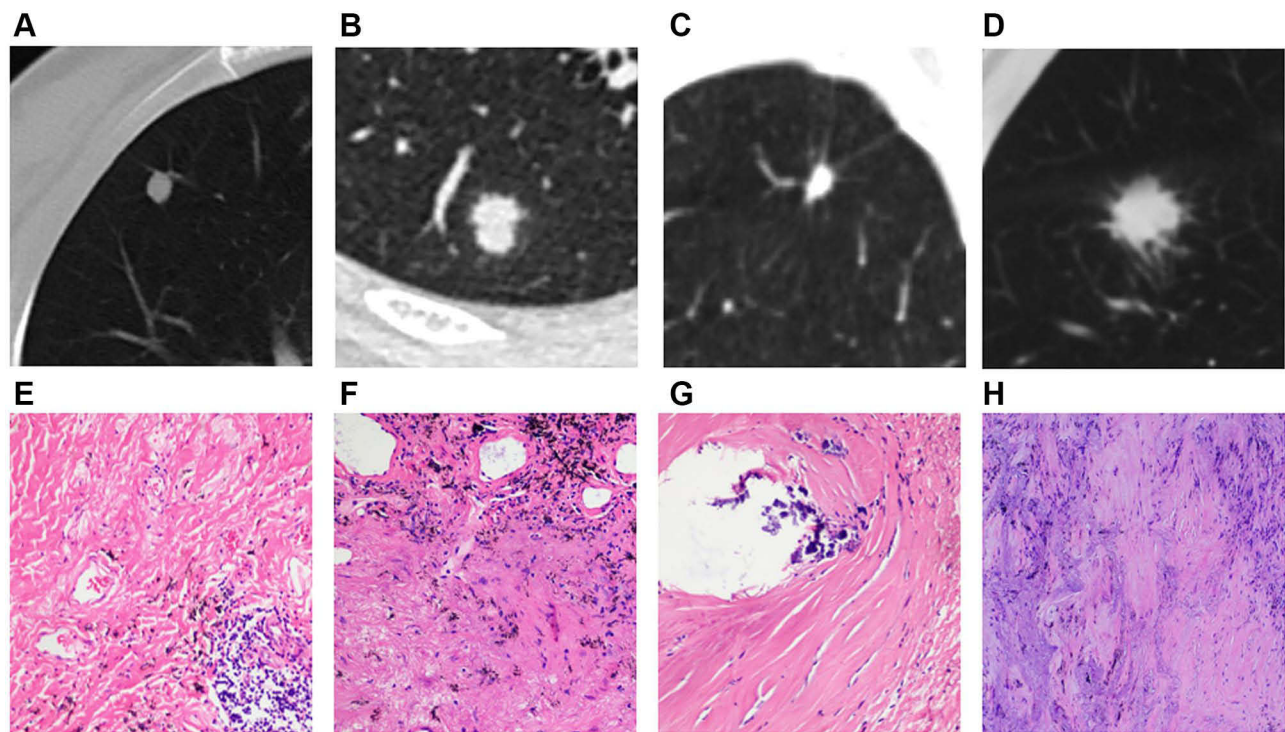


Figure 1 Solid SPINs with smooth margin (type Ia) (A), coarse margin (type Ib) (B), sparse and long spiculations (type Ic) (C), and sparse and short spiculations (type Ic) (D). Pathologically, they have similar manifestations including significant fibrous tissue proliferation, hyaline change and few chronic inflammatory cells infiltration (E–H).

and IV nodules were more common (each $P < 0.0001$) in SPINs, while the frequencies of all subtypes I ($P = 0.095$) and type III ($P = 0.796$) nodules were similar between two groups.

In the 57 type Ic SPINs, spiculations in 30 (52.6%) lesions were sparse and long, in 23 (40.4%) were sparse and short, in 3 (5.3%) were sparse, short, and long, and in 1 (1.8%) was intensive. In the 86 type Ic lung cancers, spiculations in 43 (50.0%) lesions were sparse and long, in 18 (20.9%) were sparse and short, and in 25 (29.1%) were intensive. Compared with lung cancer, sparse and short spiculations were more common ($P = 0.012$) but intensive spiculations were less common ($P < 0.0001$) in type Ic SPINs. For type II nodules, more nodules with blurred boundary (54.8% vs 10%, $P < 0.0001$) and peripheral patch (90% vs 45.2%, $P < 0.0001$) were detected in SPINs and lung cancers, respectively. Regarding nodules with peripheral patch, all of the ground glass opacities surrounded nodules (100%) and were ill-defined (100%) in SPINs (Figure 2) but those mostly located at one side of nodules (83.3%) and were always well-defined (100%) in lung cancers (Figure 5E and F). For type III nodules, the cancerous ones presented as mixed branched (Figure 5G) or reticulated (Figure 5H) higher density and peripheral

slightly lower density (Figure 5G), while these were not found in SPINs.

In SPINs, lesions with CT features of more than one type were more common than those in lung cancers (8.9% vs 1.9%, $P < 0.0001$). Compared with lung cancers, lesions abutting pleura were more common in SPINs (25.8% vs 3.5%, $P < 0.0001$), while both of them frequently had a wide base attached to pleura (70.7% vs 54.5%, $P = 0.484$). In addition, sporadic patch in same lobe (12.9% vs 4.2%, $P < 0.0001$) and intranodular calcification (4.9% vs 1.3%, $P = 0.013$) were more commonly detected in SPINs than in lung cancers, while frequencies of vacuole or cavity, pleural indentation, and air bronchogram in both groups were similar (each $P > 0.05$).

Pathological Findings of SPINs

Among the 310 cancerous nodules, 276 (89.0%) were adenocarcinomas, 23 (7.4%) were squamous carcinomas, 7 (2.3%) were neuroendocrine carcinomas, and 4 (1.3%) were adenosquamous carcinoma and mucoepidermoid carcinoma. Among the 225 SPINs, 203 (90.2%) were nonspecific inflammation (Figures 1–4), 17 (7.6%) were tuberculosis (Figure 6A–E), and 5 (2.2%) were fungal infection (Figure 6F and G). The pathological findings of

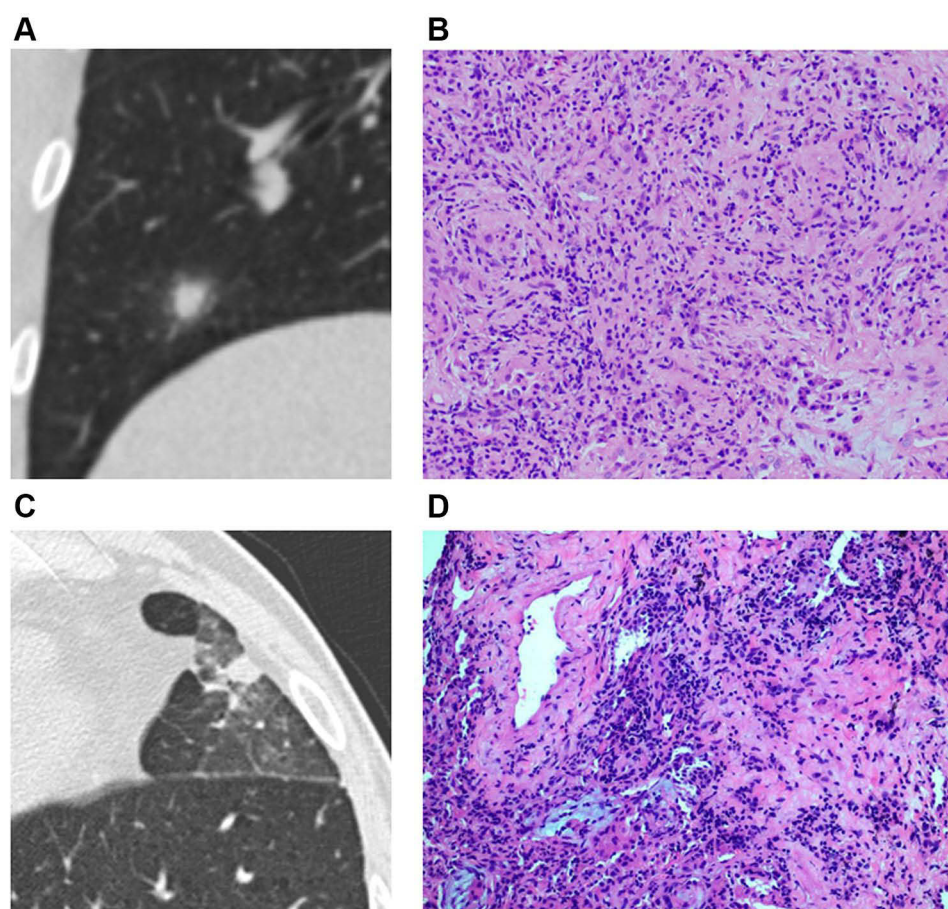


Figure 2 Solid SPINs with blurred margin (A) and peripheral patch (C) (type II). Pathologically, they have similar manifestations including more acute and chronic inflammatory cells infiltration and fibrous tissue proliferation (B and D).

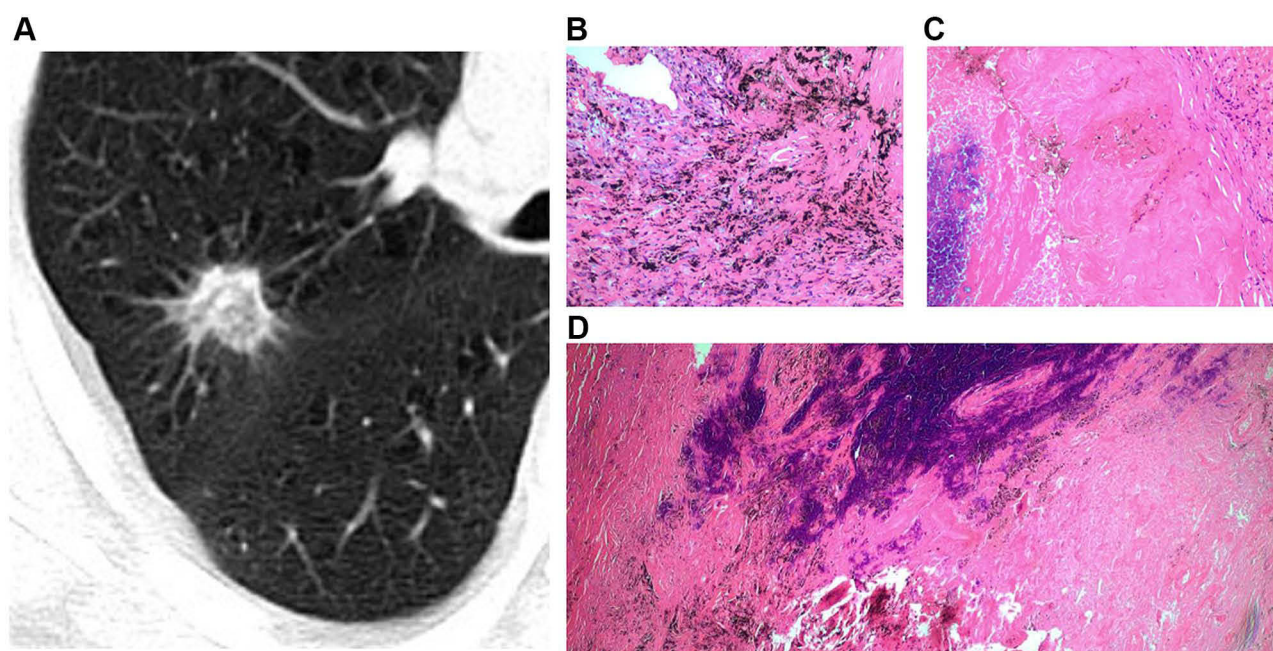


Figure 3 Solid SPIN with heterogeneous density (type III) and spiculations (A) on lung window. Pathologically, it consists of multiple components including fibrous tissue (B), hyaline change (C), calcification (D), and few inflammatory cells (B and C).

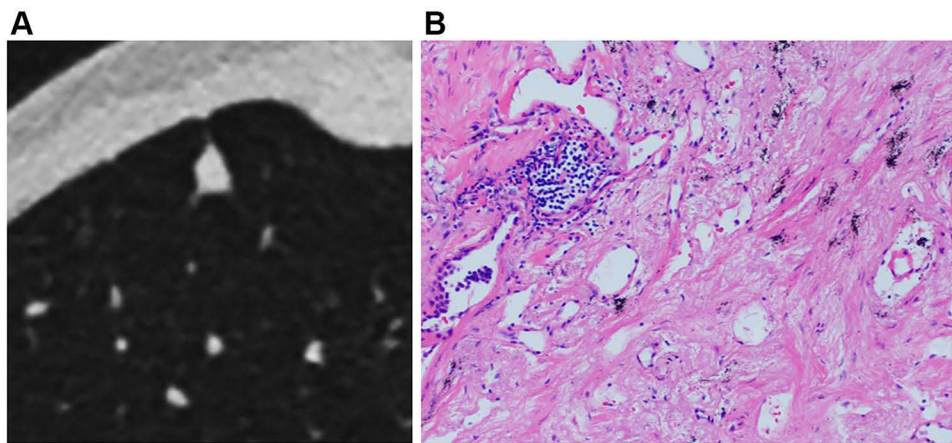


Figure 4 Solid SPIN with polygonal shape (type IV) (A). It has homogeneous density and smooth margin. Pathologically, it consists of fibrous tissue proliferation, hyaline change and a small amount of inflammatory cells infiltration (B).

SPINs are summarized in Table 4. Different types of SPINs had similar pathological components but with different predominance. In type I SPINs, fibrous tissue proliferation and hyaline change were significant, and infiltration with few chronic inflammatory cells could be detected (128, 93.5%) (Figure 1). In type II SPINs, more acute and chronic

inflammatory cells could be detected, in addition to fibrous tissue proliferation (51, 82.2%, Figure 2). In type III SPINs, multiple components could be observed: fibrous tissue proliferation, hyaline change, hemorrhage, mucoid degeneration, calcification, and inflammatory cell infiltration (12, 100%) (Figure 3). Type IV SPINs, like type I SPINs,

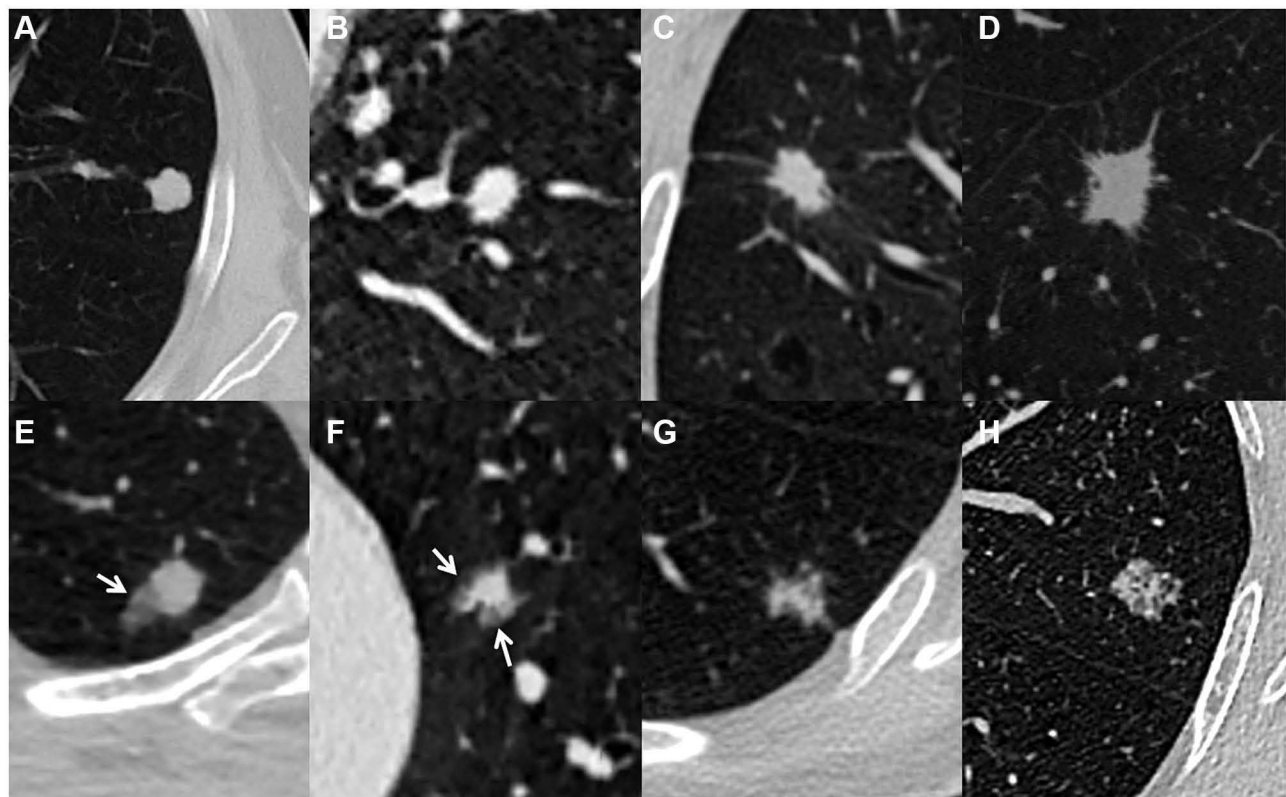


Figure 5 Solid cancerous nodules with smooth and lobulated margin (type Ia) (A), coarse margin (type Ib) (B), lobulated margin and sparse and long spiculations (type Ic) (C), intensive and short spiculations (type Id) (D), well-defined peripheral patch locating at one side (arrow) (E) or surrounding lesion (arrows) (F) (type II), and heterogeneous density (type III) (G and H).

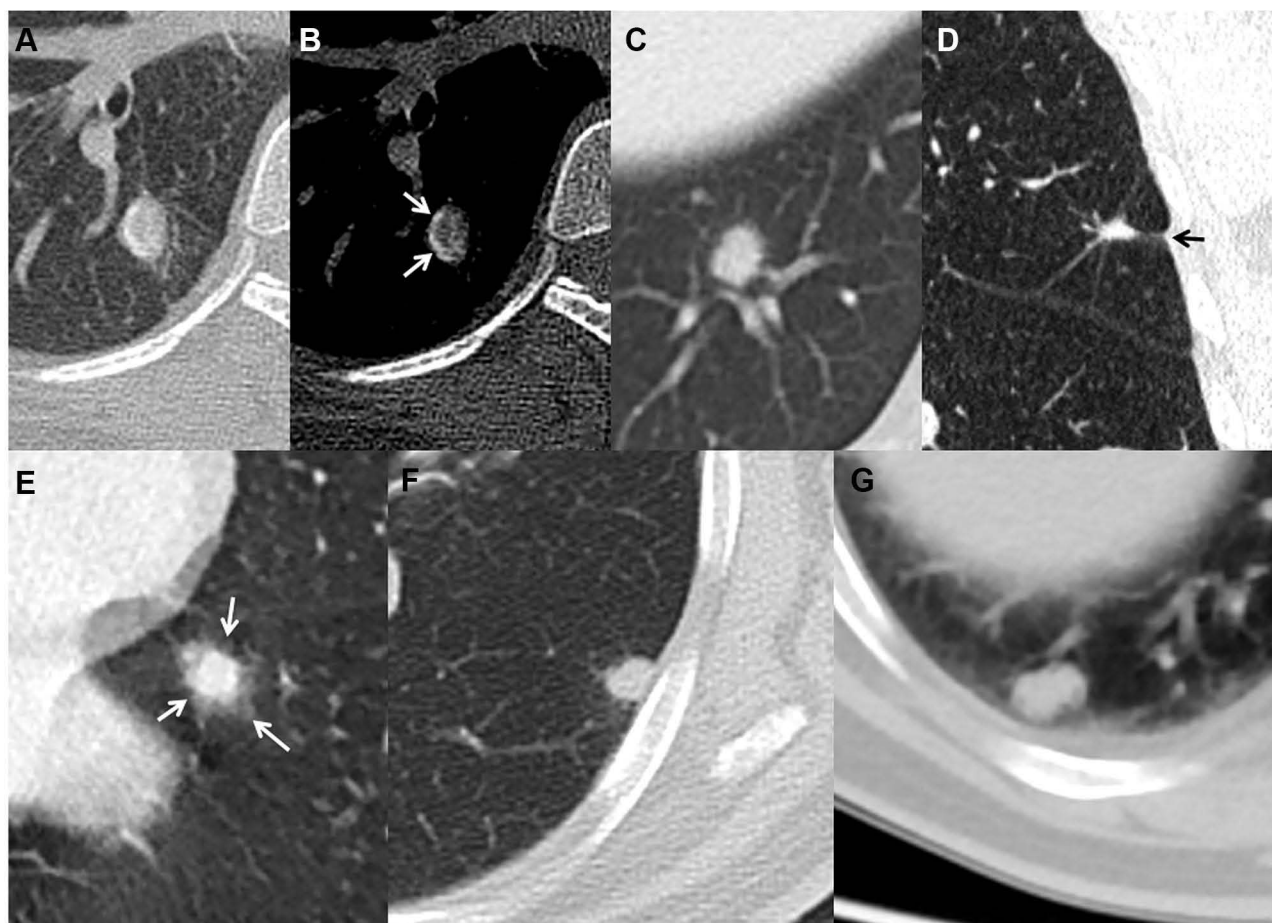


Figure 6 Tuberculous nodules with smooth margin (A) and curved calcification (arrows) (B), coarse margin (C), sparse and long spiculations and pleural indentation (arrow) (D), and ill-defined peripheral patch (arrows) (E). A cryptococcal nodule abutting pleura with a wide base (F), and an oval aspergillus nodule with clear and smooth margin (G).

exhibited fibrous tissue proliferation, hyaline change, and infiltration with few chronic inflammatory cells (14, 100%) (Figure 4).

Discussion

In this study, solid SPINs exhibited various CT manifestations and some were exclusive, whereas each type had relatively uniform pathological findings. Knowing the pathological characteristics of SPINs as well is helpful for understanding their different CT manifestations. However, CT features for each type were not distinct; different SPINs had CT manifestations of more than one type. Moreover, some types of SPINs also had signs that could be found in lung cancers. Thus, a further understanding the potential differences in their CT features is needed.

With regard to lesion distribution and location, SPINs were found mainly in the superior lobe, which was similar

to the location of lung cancers in this and previous studies.¹⁶ Some SPINs in this study were closely attached to adjacent pleura and a majority of those had a wide base, while these were rare for lung cancers.^{4–6,17–20} Peripheral inflammation frequently involving distal subpleural lung tissues may account for these differences. For nodules not abutted pleura, pleural indentations were all infrequent and similar in SPIN and lung cancer group. Thus, pleural indentation could not be used for differentiating them.

Compared with lung cancers, irregular nodules were relatively common but lobulated ones were infrequent in SPIN group. This may be related to the proliferation of fibrosis and infiltration of inflammatory cells in SPINs rather than the concurrence of different rates of cell growth and restriction caused by adjacent interstitium in lung cancers.^{4,11,16,21–23} Additionally, a few nodules with flat edges manifesting as polygonal shapes were only found in SPINs, which was probably caused by obstruction of

Table 4 The Pathological Findings of SPINs

Main Pathological Findings	Number	Percentage (%)
Type 1	137	
Significant fibrous tissue + few inflammatory cells	82	59.9
Significant fibrous tissue + hyaline change + few inflammatory cells ± calcification	46 (7*)	33.6
Significant fibrous tissue + more inflammatory cells	9	6.6
Type 2	62	
More inflammatory cells + fibrous tissue	34	54.8
Massive inflammatory cells + fibrous tissue	17	27.4
Fibrous tissue + few inflammatory cells	11	17.7
Type 3	12	
Fibrous tissue + hyaline change + calcification + hemorrhage + few inflammatory cells	7	58.3
Fibrous tissue + hyaline change + mucoid degeneration + few inflammatory cells	5	41.7
Type 4	14	
Fibrous tissue proliferation + few inflammatory cells	10	71.4
Fibrous tissue + hyaline change + few inflammatory cells	4	28.6

Note: *Number of cases with calcification.

adjacent structures. Thus, lobulated sign and polygonal shapes are meaningful for discriminating solid nodules.

Heterogeneous attenuation can be detected in both inflammatory and malignant nodules, but different pathological processes are responsible for this appearance.^{5,9,12} Heterogeneous SPINs usually had multiple pathological components; however, the heterogeneous density in solid cancerous nodules usually indicated degeneration or uneven distribution of tumor cells.¹⁹ In lung cancers, heterogeneous lesions would become homogeneous as growing due to tumor cell proliferation, but this change would not happen in inflammatory nodules.^{19,24–26} Therefore, follow-up for monitoring density change is useful for differentiating heterogeneous nodules.

Spiculations are closely associated with lung cancers.^{2,4,8,12,16} However, the present study showed the occurrences of nodules with spiculations were similar in both groups but their CT features were different. The intensive spiculations were almost only found in lung cancers, while sparse and short ones were frequently detected in SPINs. These differences may be due to the hyperplasia of fibrous tissue and infiltration of inflammatory cells or tumor cells. Therefore, nodules with intensive spiculations were more likely to be tumor, and other CT features should be considered for differentiating nodules with other patterns of spiculations.

The halo sign (HS) can be seen in a large number of diverse conditions, which is the radiological correlate of infiltration (hemorrhage, neoplastic or inflammatory).²⁷ In the present study, both the SPINs and lung cancers showed this sign but they were different. The HS (peripheral patch) in SPINs was ill-defined while most of that in lung cancers was well-defined, which was consistent with previous results.^{28–30} The pathological findings revealed that ill-defined HS detected in SPINs was closely related to the infiltration of massive inflammatory cells. Moreover, sporadic patches were detected in the same lobe with SPINs in some cases, which may be additional evidence of SPINs. Therefore, blurred boundaries and ill-defined peripheral patches are more typical of SPINs and this help distinguish them from lung cancers.

Regarding other CT characteristics, intranodular calcification was more commonly detected in SPINs than in lung cancers, while frequencies of vacuole or cavity, pleural indentation, and air bronchogram in both groups were similar. Compared with previous studies, the calcification in SPINs was far less common than that in benign nodules,^{2,4} but it was a potential sign for evaluating nodule and distinguishing them.

This study had several limitations. First, the key CT features for dividing SPINs into different types were not exclusive; some SPINs had features of more than one type. In addition, some SPINs and lung cancers (such as types I and III) shared same CT features, which still could not be well differentiated. However, after studying the pathological findings, it revealed that types I and III SPINs may not grow significantly due to significant fibrous tissue proliferation and hyaline change. Thus, follow-up could provide more information for the likely diagnosis because most of malignant solid nodules will increase in size and/or density,³¹ and such information should be added in an affected patient's flowchart for discriminating SPINs from cancerous nodules.

In conclusion, SPINs share different CT features that are closely correlated with pathological findings. There are differences in overall or specific CT features between cancerous nodules and SPINs. Solid pulmonary nodules should be highly suspected of being inflammatory nodules if they have blurred boundaries, peripheral patches, or polygonal shapes on CT images. In contrast, nodules with intensive spiculations or lobulated sign have a high possibility of malignancy. For nodules without distinct CT features, follow-up may be helpful for discriminating by monitoring changes related to different pathological bases.

Ethics Statement

The study was conducted in accordance with the Declaration of Helsinki, and the protocol was approved by the Ethics Committee of The First Affiliated Hospital of Chongqing Medical University (No. 2019-062), which absolved the need for written informed consent because of the retrospective study. All personal identification data were anonymized and de-identified before analysis.

Funding

This study was supported by the National Natural Science Foundation of China (81601545) and Chongqing Health and Family Planning Commission Foundation (2016MSXM018) of China.

Disclosure

The authors report no conflicts of interest in this work.

References

- Choi SM, Heo EY, Lee J, et al. Characteristics of benign solitary pulmonary nodules confirmed by diagnostic video-assisted thoracoscopic surgery. *Clin Respir J*. 2016;10:181–188. doi:10.1111/crj.12200
- Erasmus JJ, Connolly JE, McAdams HP, Roggli VL. Solitary pulmonary nodules: Part I. Morphologic evaluation for differentiation of benign and malignant lesions. *Radiographics*. 2000;20:43–58. doi:10.1148/radiographics.20.1.g00ja0343
- Hodnett PA, Ko JP. Evaluation and management of indeterminate pulmonary nodules. *Radiol Clin North Am*. 2012;50:895–914. doi:10.1016/j.rcl.2012.06.005
- Snoeckx A, Reyntiens P, Desbuquoit D, et al. Evaluation of the solitary pulmonary nodule: size matters, but do not ignore the power of morphology. *Insights Imaging*. 2018;9:73–86. doi:10.1007/s13244-017-0581-2
- Zwirewich CV, Vedal S, Miller RR, Müller NL. Solitary pulmonary nodule: high-resolution CT and radiologic-pathologic correlation. *Radiology*. 1991;179:469–476. doi:10.1148/radiology.179.2.2014294
- Li BG, Ma DQ, Xian ZY, et al. The value of multislice spiral CT features of cavity walls in differentiating between peripheral lung cancer cavities and single pulmonary tuberculous thick-walled cavities. *Br J Radiol*. 2012;85:147–152. doi:10.1259/bjr/79051309
- Honda O, Tsubamoto M, Inoue A, et al. Pulmonary cavity nodules on computed tomography: differentiation of malignancy and benignancy. *J Comput Assist Tomogr*. 2007;31:943–949. doi:10.1097/RCT.0b013e3180415e20
- Sim YT, Poon FW. Imaging of solitary pulmonary nodule—a clinical review. *Quant Imaging Med Surg*. 2013;3:316–326. doi:10.3978/j.issn.2223-4292.2013.12.08
- Park CM, Goo JM, Lee HJ, Lee CH, Chun EJ, Im JG. Nodular ground-glass opacity at thin-section CT: histologic correlation and evaluation of change at follow-up. *Radiographics*. 2007;27:391–408. doi:10.1148/rg.272065061
- Nambu A, Araki T, Taguchi Y, et al. Focal area of ground-glass opacity and ground-glass opacity predominance on thin-section CT: discrimination between neoplastic and non-neoplastic lesions. *Clin Radiol*. 2005;60:1006–1017. doi:10.1016/j.crad.2005.06.006
- Qiu ZX, Cheng Y, Liu D, et al. Clinical, pathological, and radiological characteristics of solitary ground-glass opacity lung nodules on high-resolution computed tomography. *Ther Clin Risk Manag*. 2016;12:1445–1453. doi:10.2147/TCRM.S110363
- Borghesi A, Michelini S, Nocivelli G, et al. Solid indeterminate pulmonary nodules less than or equal to 250 mm³: application of the updated Fleischner society guidelines in clinical practice. *Radiol Res Pract*. 2019;2019:7218258. doi:10.1155/2019/7218258
- Gould MK, Fletcher J, Lannetoni MD, et al. Evaluation of patients with pulmonary nodules: when is it lung cancer? ACCP evidence-based clinical practice guidelines (2nd edition). *Chest*. 2007;132:108S–130S. doi:10.1378/chest.07-1353
- Satoh S, Kitazume Y, Ohdama S, Kimura Y, Taura S, Endo Y. Can malignant and benign pulmonary nodules be differentiated with diffusion-weighted MRI? *AJR Am J Roentgenol*. 2008;191:464–470. doi:10.2214/AJR.07.3133
- You X, Sun X, Yang C, Fang Y. CT diagnosis and differentiation of benign and malignant varieties of solitary fibrous tumor of the pleura. *Medicine*. 2017;96:e9058. doi:10.1097/MD.00000000000009058
- Chu ZG, Sheng B, Liu MQ, Lv FJ, Li Q, Ouyang Y. Differential diagnosis of solitary pulmonary inflammatory lesions and peripheral lung cancers with contrast-enhanced computed tomography. *Clinics*. 2016;71:555–561. doi:10.6061/clinics/2016(10)01
- Xu C, Hao K, Song Y, Yu L, Hou Z, Zhan P. Early diagnosis of solitary pulmonary nodules. *J Thorac Dis*. 2013;5:830–840. doi:10.3978/j.issn.2072-1439.2013.11.19
- Li M, Ito H, Wada H, Tanaka F. Pit-fall sign on computed tomography predicts pleural involvement and poor prognosis in non-small cell lung cancer. *Lung Cancer*. 2004;46:349–355. doi:10.1016/j.lungcan.2004.05.017
- Yang ZG, Sone S, Takashima S, et al. High-resolution CT analysis of small peripheral lung adenocarcinomas revealed on screening helical CT. *AJR Am J Roentgenol*. 2001;176:1399–1407. doi:10.2214/ajr.176.6.1761399
- Hsu JS, Jaw TS, Yang CJ, et al. Convex border of peripheral non-small cell lung cancer on CT images as a potential indicator of pleural invasion. *Medicine*. 2017;96:e7323. doi:10.1097/MD.00000000000007323
- Fan L, Liu SY, Li QC, Yu H, Xiao XS. Multidetector CT features of pulmonary focal ground-glass opacity: differences between benign and malignant. *Br J Radiol*. 2012;85:897–904. doi:10.1259/bjr/33150223
- Gurney JW, Lyddon DM, McKay JA. Determining the likelihood of malignancy in solitary pulmonary nodules with Bayesian analysis. Part II. Application. *Radiology*. 1993;186:415–422. doi:10.1148/radiology.186.2.8421744
- Wang YX, Gong JS, Suzuki K, Morcos SK. Evidence based imaging strategies for solitary pulmonary nodule. *J Thorac Dis*. 2014;6:872–887. doi:10.3978/j.issn.2072-1439.2014.07.26
- Chu ZG, Zhang Y, Li WJ, Li Q, Zheng YN, Lv FJ. Primary solid lung cancerous nodules with different sizes: computed tomography features and their variations. *BMC Cancer*. 2019;19(1):1060. doi:10.1186/s12885-019-6274-0

25. Xu DM, van Klaveren RJ, de Bock GH, et al. Role of baseline nodule density and changes in density and nodule features in the discrimination between benign and malignant solid indeterminate pulmonary nodules. *Eur J Radiol.* 2009;70:492–498. doi:10.1016/j.ejrad.2008.02.022
26. Oda S, Awai K, Murao K, et al. Volume-doubling time of pulmonary nodules with ground glass opacity at multidetector CT: assessment with computer-aided three-dimensional volumetry. *Acad Radiol.* 2011;18:63–69. doi:10.1016/j.acra.2010.08.022
27. Ray A, Mittal A, Vyas S. CT Halo sign: a systematic review. *Eur J Radiol.* 2020;124:108843. doi:10.1016/j.ejrad.2020.108843
28. Pinto PS. The CT Halo sign. *Radiology.* 2004;230:109–110. doi:10.1148/radiol.2301020649
29. Kim HY, Shim YM, Lee KS, Han J, Yi CA, Kim YK. Persistent pulmonary nodular ground-glass opacity at thin-section CT: histopathologic comparisons. *Radiology.* 2007;245:267–275. doi:10.1148/radiol.2451061682
30. Aoki T, Nakata H, Watanabe H, et al. Evolution of peripheral lung adenocarcinomas: CT findings correlated with histology and tumor doubling time. *AJR Am J Roentgenol.* 2000;174:763–768. doi:10.2214/ajr.174.3.1740763
31. Zhang R, Tian P, Qiu Z, Liang Y, Li W. The growth feature and its diagnostic value for benign and malignant pulmonary nodules met in routine clinical practice. *J Thorac Dis.* 2020;12(5):2019–2030. doi:10.21037/jtd-19-3591

Journal of Inflammation Research

Dovepress

Publish your work in this journal

The Journal of Inflammation Research is an international, peer-reviewed open-access journal that welcomes laboratory and clinical findings on the molecular basis, cell biology and pharmacology of inflammation including original research, reviews, symposium reports, hypothesis formation and commentaries on: acute/chronic inflammation; mediators of inflammation; cellular processes; molecular

mechanisms; pharmacology and novel anti-inflammatory drugs; clinical conditions involving inflammation. The manuscript management system is completely online and includes a very quick and fair peer-review system. Visit <http://www.dovepress.com/testimonials.php> to read real quotes from published authors.

Submit your manuscript here: <https://www.dovepress.com/journal-of-inflammation-research-journal>